that this angle is 148° for triplet DPC.[15] Singlet methylene prefers a small bond angle of 102°, and the singlet energy climbs rapidly upon increasing this angle. Triplet methylene has a bond angle of 138°.[32] The large angles observed for DPC are a consequence of steric repulsion. This selectively raises the singlet energy and increases ΔE_{ST}. The situation is reversed in fluorenylidene, where molecular architecture enforces a small angle, favoring the singlet and lowering the singlet–triplet gap.

The activation energies of Table II are much smaller than those predicted from low-temperature ESR kinetic data which have been fit to an asymmetric Eckart barrier. This could be due to the problem of site inequivalence in the matrix leading to an oversimplified interpretation. Alternatively, one may be looking at reaction trajectories in the matrix that are not ideal, as they may be in solution. This would require the matrix reaction to overcome a larger barrier than the solution process.

The activation energies of Table II are only slightly smaller than the ab initio calculations of Schaeffer for the prototypical reaction,

$$^3CH_2 + CH_4 \rightarrow 2CH_3\cdot \qquad E_a(\text{calcd}) = 7 \text{ kcal/mol}$$

and very much smaller than the barriers calculated by semiempirical methods.[33] The small discrepancy between theory and experiment may be due to an invalid comparison between different carbenes, or to artificially low experimental activation energies (vide infra).

The experimental Arrhenius parameters were determined from the radical growth lifetimes in solution. Side reactions (such as azine formation or reaction with traces of water or oxygen) may become more prevalent at low temperatures. Under these conditions the observable Arrhenius parameters could be lower than those for the abstraction reaction itself.

Experimental Section

Diphenyldiazomethane was prepared according to a literature procedure[34] and purified by sublimation under vacuum. The solvents were purified by standard procedures or used as received when spectrograde solvents were commercially available.

Deaerated samples for the laser photolysis experiments were either contained in or flowed through cells made of 7 × 7 mm² square Suprasil tubing. An excimer laser (Lumonics Model TE-860-2) operated with Xe/HCl/He mixtures was used for excitation at 308 nm (~4 ns, up to 80 mJ/pulse). The detection system employed a Tektronix R-7912 transient digitizer to capture the signals that are then transferred to a PDP 11/23 computer which controls the experiment and provides suitable processing, storage, and hardcopy facilities. Further details have been given elsewhere.[35]

Acknowledgment. The authors are indebted to Mr. S. E. Sugamori for technical assistance.

Registry No. Diphenyldiazomethane, 883-40-9; diphenylcarbene, 3129-17-7; cyclohexane, 110-82-7; toluene, 108-88-3; tetrahydrofuran, 109-99-9; cyclohexene, 110-83-8; methylcyclohexane, 108-87-2; 2-methyltetrahydrofuran, 96-47-9; triethylamine, 121-44-8; cyclopentane, 287-92-3; 1-octene, 111-66-0; cyclooctene, 931-88-4; 2,3-dimethyl-2-butene, 563-79-1; styrene, 100-42-5; 1,4-cyclohexadiene, 628-41-1; 1,3-cyclohexadiene, 592-57-4; 1,5-cyclooctadiene, 111-78-4; 1,3-cyclooctadiene, 1700-10-3; 1,3-octadiene, 1002-33-1; chloroform, 67-66-3; deuterium, 7782-39-0; hydrogen, 1333-74-0; chlorine, 7782-50-5; diphenylmethyl, 4471-17-4; carbon tetrachloride, 56-23-5.

(32) (a) Pople, J. A.; Binkley, J. S.; Seegen, R. *Int. J. Quantum Chem.* **1976**, *104*, 1. (b) Harding, L. B.; Goddard, W. A. III *Chem. Phys. Lett.* **1978**, *55*, 217. (c) Shih, S.-K.; Peyerimhoff, S. D.; Buenker, R. J.; Peric, M. *Ibid.* **1978** *55*, 206. (d) Bauschlicher, C. W., Jr.; Shavitt, I. *J. Am. Chem. Soc.* **1978**, *100*, 739. (e) Lucchese, R. R.; Schaefer, H. F., III *Ibid.* **1977**, *99*, 6765. (f) For earlier theoretical treatments of methylene, see: Harrison, J. F. *Acc. Chem. Res.* **1974**, *7*, 378. (g) Zittel, P. F.; Ellison, G. B.; O'Neill, S. V.; Herbst, E.; Lineberger, W. C.; Reinhardt, W. P. *J. Am. Chem. Soc.* **1976**, *98*, 3731.

(33) (a) Bauschlicher, C. N., Jr.; Bender, C. F.; Schaeffer, H. F., III *J. Am. Chem. Soc.* **1976**, *98*, 3072; see also: (b) Carr, R. W. *J. Phys. Chem.* **1972**, *76*, 1581. (c) Bodor, N.; Dewar, M. J. S.; Wasson, J. S. *J. Am. Chem. Soc.* **1972**, *94*, 9095.

(34) Smith, L. I.; Howard, K. L. "Organic Synthesis"; Collect Vol. III; Wiley: New York, 1955; p 351.

(35) Scaiano, J. C. *J. Am. Chem. Soc.* **1980**, *102*, 7747–7753.

Single-Crystal Polarized Electronic Absorption Spectrum and Ligand-Field Interpretation of the Bonding of Zeise's Salt

Tsu-Hsin Chang and Jeffrey I. Zink*

Contribution from the Department of Chemistry, University of California, Los Angeles, Los Angeles, California 90024. *Received May 9, 1983*

Abstract: The single-crystal polarized spectra of Zeise's salt, $K[Pt(C_2H_4)Cl_3]H_2O$, taken at 10 K are reported. Ligand field and charge-transfer transitions are assigned. The vibronic structure is assigned and excited-state distortions are interpreted. Angular overlap parameters for the ligands are determined. Ethylene is a strong σ donor and a very weak π acceptor toward Pt(II). The relevance of the excited-state assignments to the photochemical reactivity of Zeise's salt is discussed.

Zeise's salt, $K[Pt(C_2H_4)Cl_3]H_2O$, is one of the most intensively studied compounds containing a metal–olefin bond.[1] The Dewar–Chatt model is generally accepted as providing the best description of the metal–olefin interaction.[2,3] The interaction is considered to consist of a σ bond in which the filled π-bonding orbital of the olefin donates electrons to an empty metal d orbital, and a π back-bond in which a filled metal d orbital donates electrons to an empty π-antibonding orbital on the olefin. The relative importance of the σ and π components is still a topic of discussion (vide infra).

Four types of molecular orbital calculations have been performed on Zeise's salt, yielding different interpretations of the metal–olefin bonding. In an extended Hückel calculation,[4] a CNDO type calculation,[5] and an ab initio calculation[6] the σ and π components were calculated to be about equal. A recent $X\alpha$-SW SCF calculation[7] suggested that the σ bonding components are

(1) Zeise, W. C.; Pogg *Liebigs Ann. Chem.* **1831**, *21*, 477. See also: Cotton, F. A.; Wilkinson, G. "Advanced Inorganic Chemistry", 4th ed.; Wiley: New York, 1980.

(2) Dewar, M. J. S. *Bull. Soc. Chim. Fr.* **1951**, *18*, C79.

(3) Chatt, J.; Duncanson, L. A. *J. Chem. Soc.* **1953**, 2939.

(4) Moore, J. W. *Acta Chem. Scand.* **1966**, *20*, 1154.

(5) Kato, H. *Bull. Chem. Soc. Jpn.* **1971**, *44*, 348.

(6) Hay, P. J. *J. Am. Chem. Soc.* **1981**, *103*, 1390.

(7) Rosch, N.; Messmer, R. P.; Johnson, K. H. *J. Am. Chem. Soc.* **1974**, *96*, 3855.

0002-7863/84/1506-0287$01.50/0

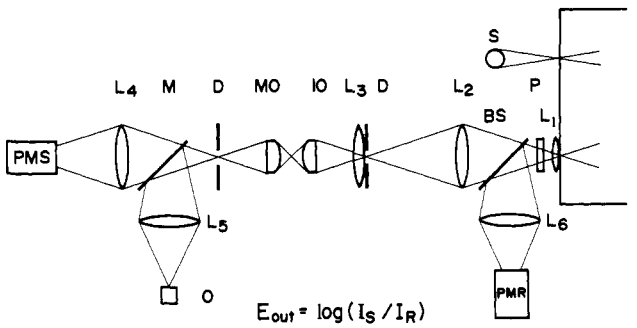

Figure 1. Block diagram of the absorption spectrometer. The output of a 150-W xenon lamp source (S) is passed through a 1-m monochrometer. The monochromatic light passes through focussing lenses L_1 through L_6, a Glan–Thompson polarizer (P), a beam splitter (BS), right-angle diaphragms (D), and two quartz microscope objectives (MO). The light is either observed visually by using the swing-away mirror (M) and a microscope ocular (O) or is detected by the sample photomultiplier (PMS) and the reference photomultiplier (PMR).

considerably more important than the π back-bonding.

The d-orbital ordering in square-planar complexes in general and Zeise's salt in particular has also been the subject of current discussion. The molecular orbital calculations gave different results. Solution spectroscopic studies have also been carried out, yielding still another order.[8]

In this paper we report spectroscopically determined σ and π metal–olefin bonding properties. The single-crystal polarized absorption spectrum of Zeise's salt is measured and assigned. Both the ligand field absorption bands and the low-lying metal–ligand charge-transfer bands are assigned. The d orbital ordering is determined. Ligand field parameters are calculated for the olefin ligand for the first time, and the angular overlap σ and π parameters are calculated and interpreted in terms of the bonding components of the Dewar–Chatt model. The vibronic structure is interpreted and the excited-state distortions are calculated. The relationship between the bonding properties of the excited states and the photochemical reactions are discussed.

Experimental Section

The major impediment to the measurement of absorption spectra of organometallic compounds has been the large molar absorptivities of the absorption bands in these compounds. An obvious method of circumventing this problem is the use of extremely thin crystals of the compound of interest. Unless crystals of the desired thinness can be cleaved from larger crystals (a difficult or impossible task with soft organometallic molecular crystals), the crystals must be grown directly on an optically transmitting support. Thin crystals of Zeise's salt were grown between quartz plates in the dark by slow evaporation of concentrated aqueous solutions. The crystals obtained were generally on the order of tens of micrometers in length and breadth.

In order to measure the absorption spectra of oriented microcrystals, an instrument was locally constructed around microscope objectives as the final optical elements.[9] A schematic diagram of the instrument is shown in Figure 1. The output of a 150-W xenon arc lamp was passed through a 1-m Bausch and Lomb scanning monochromator with slit widths less than 2 mm. Polarized light was obtained with a Halle Glan–Thompson polarizer having an extinction of 10^{-5}. The light passed through focusing optics having Zeiss 10X quartz microscope objectives as the final elements. The light was split into two components. Both the reference detector and the sample detector were EMI 9558 Q photomultiplier tubes. The logarithm of the ratio of the sample and reference detector signals was obtained with an analog circuit. The output was fed to a locally constructed A/D converter and the digitized spectrum stored and worked up in a PDP 11/02 microprocessor. The sample was cooled by an Air Products displex closed cycle cryogenic cooler.

An important feature of the instrument is the ability to visually observe and align the sample by using the swing-away mirror and microscope ocular shown in Figure 1. With the mirror in place, the microcrystal is observed under 100× magnification. The crystal is aligned, an optically clear and smooth region is chosen for measurement, and the front and rear right-angle diaphragms are closed to monitor only the desired part of the crystal and to reject stray light. After alignment is complete, the mirror is swung out of the optical path and the spectrum is recorded.

Zeise's salt was synthesized according to the literature method.[10] Single crystals were grown between 6-mm-diameter quartz plates by slow evaporation in the dark of concentrated aqueous solutions. Crystals having approximate dimensions of 20 × 40 μm with well-defined edges and extinction properties under the polarizing microscope were chosen for study.

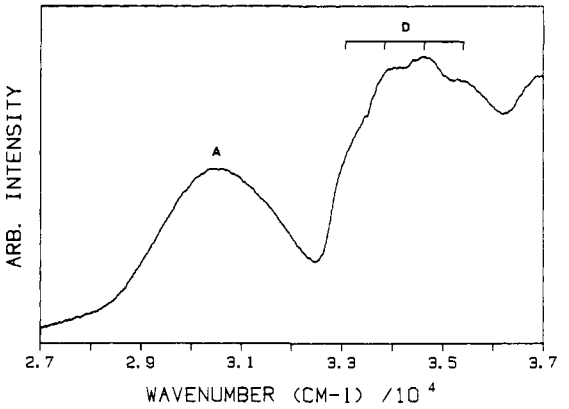

Figure 2. Absorption spectrum of a single crystal of Zeise's salt at 10 K polarized perpendicular to the crystallographic c axis.

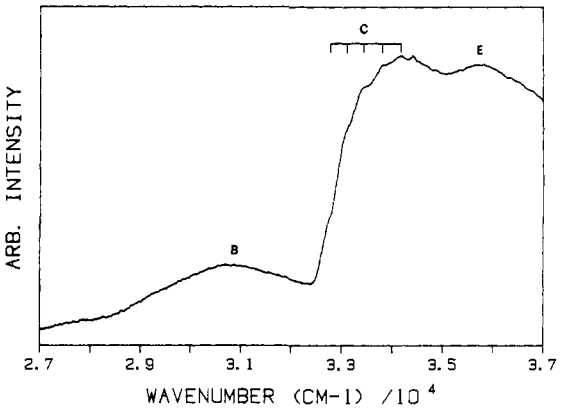

Figure 3. Absorption spectrum of the same single crystal whose spectrum is shown in Figure 1 polarized parallel to the crystallographic c axis.

Table I. Peak Maxima and Assignments

absorption maximum, cm^{-1}	polarization	assignment	label in Figures 1 and 2
30 313	$\perp$	$^1B_1\ xy \rightarrow x^2-y^2$	A
31 238	b	$^1A_2\ yz \rightarrow x^2-y^2$	B
34 118	$\parallel$	$^1B_2\ xz \rightarrow x^2-y^2$	C
34 600	$\perp$	$^3A_2\ xy \rightarrow \pi^*$	D
35 739	$\parallel$	$^3B_1\ yz \rightarrow \pi^*$	E

[a] $\perp = x,y$ polarized; $\parallel = z$ polarized. [b] The polarization cannot be unambiguously determined.

Results

The electronic absorption spectra of single crystals of Zeise's salt obtained at 10 K are shown in Figures 2 and 3. The parallel spectrum was obtained with the electric vector of the incident radiation parallel to the extinction direction at an angle of 15° to the long crystal axis, which is assumed to be the crystallographic c axis. The parallel spectrum is primarily the z-polarized spectrum in the molecular axis system (vide infra). The perpendicular spectrum was obtained in the orthogonal extinction direction perpendicular to the c axis and contains primarily the x and/or

(8) Denning, R. G.; Hartley, F. R.; Venanzi, L. M. *J. Chem. Soc.* **1967**, 1322.

(9) Yerson, H.; Glieman, G. *Messtechnik (Braunschweig)* **1972**, *80*, 99.

(10) Cramer, R. *Inorg. Chem.* **1965**, *4*, 445.

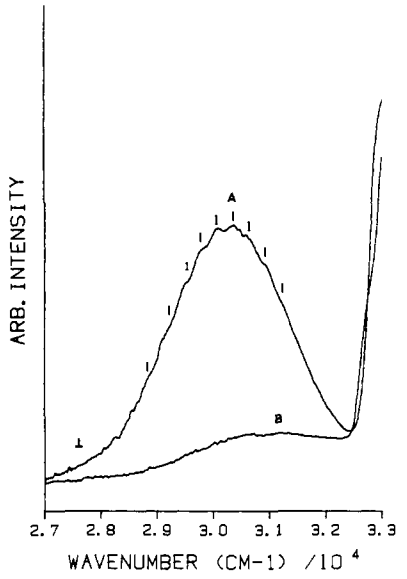

Figure 4. Absorption spectrum of the $^1A_1 \rightarrow {}^1B_1$, $xy \rightarrow x^2-y^2$ transition (band A) of Zeise's salt at 10 K. Shoulder B is the $^1A_1 \rightarrow {}^1B_1$, $yz \rightarrow x^2-y^2$ transition. Band A is $\perp$ (xy) polarized.

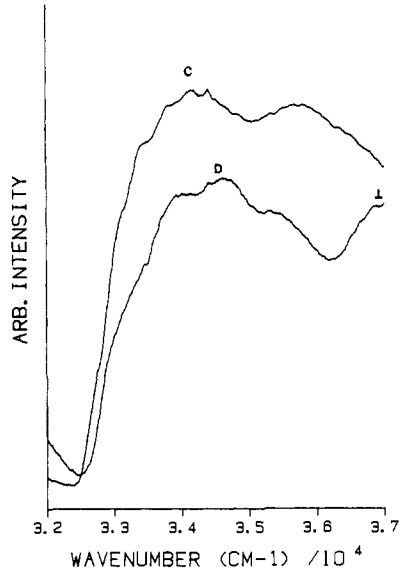

Figure 5. Absorption spectrum of the 32 000-37 000-cm^{-1} region of Zeise's salt at 10 K. Band C is the $^1A_1 \rightarrow {}^1B_2$, $xz \rightarrow x^2-y^2$ transition. The remaining transitions are metal to olefin charge-transfer transitions.

y molecular axes (vide infra). The positions of the peaks and shoulders given in Table I are labeled by using the letters shown in Figures 2 and 3.

Vibronic structure was observed in many of the absorption peaks. The longest vibronic progression occurred on the peak centered at 30 313 cm^{-1} under perpendicular polarization. At least five components were clearly discernible on the enlarged spectra shown in Figure 4. The most highly resolved vibronic peaks were those found on the peak centered at 34 600 cm^{-1} shown in Figure 5. Three well-resolved peaks and one distinct shoulder were observed. Vibronic progressions consisting of three or more members are listed in Table II.

Discussion

1. Group Theoretical Analysis. Zeise's salt forms monoclinic crystals, space group $P2_1/c$, with two formula units in the unit cell.[11] The deviations from ideal symmetry are small. In the following analysis, the compound will be assumed to have C_{2v} symmetry. The axis system which will be used is a "chemists'" axis system with the z axis perpendicular to the square plane and parallel to the ethylene. The symmetries of the platinum d orbitals and the olefin π-antibonding orbital along with the symmetries of the one-electron excited states are shown in Figure 6.

(11) (a) Jarvis, J. A. J.; Kilbourne, B. T.; Owston, P. G. *Acta Crystallogr., Sect. B* **1970**, *26*, 876; **1971**, *27*, 366. (b) Love, R. A.; Koetzle, T. F.; Williams, G. J. B.; Andrew, L. C.; Bau, R. *Inorg. Chem.* **1975**, *14*, 2653.

Table II. Positions of Vibronic Structure

band	vibronic max, cm^{-1}	sepn, cm^{-1}	band	vibronic max, cm^{-1}	sepn, cm^{-1}
$^1B_1$	28 631	304	$^1B_2$	32 732	
	28 935	304		33 079	347
	29 224	289		33 430	351
	29 514	290		33 779	349
	29 796	282		34 124	345
	30 060	264			av 348
	30 364	304	$^3A_2$	33 075	
	30 661	297		33 867	792
	30 959	298		34 653	786
	31 255	296		35 439	786
	31 559	304			av 788
	31 851	292			
		av 293			

Table III. Selection Rules

transition	polarization $\parallel(z)$	$\perp(x)$	$\perp(y)$
$^1A_1 \rightarrow {}^1A_1$	vibronic	dipole, vibronic	vibronic
$^1A_1 \rightarrow {}^1A_2$	vibronic	forbidden	vibronic
$^1A_1 \rightarrow {}^1B_1$	forbidden	vibronic	dipole, vibronic
$^1A_1 \rightarrow {}^1B_2$	dipole, vibronic	vibronic	forbidden

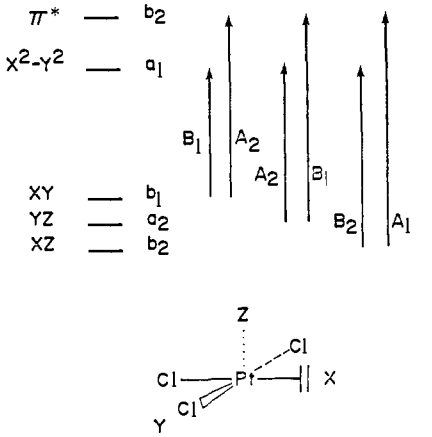

Figure 6. Axis system, orbital symmetries, and excited-state symmetries for Zeise's salt.

The electronic selection rules are summarized in Table III. The x, y, and z components of the electric dipole operator transform as a_1, b_1, and b_2, respectively. Spin-allowed transitions that are allowed or forbidden by the electric dipole operator are called dipole transitions here. For the vibronic transitions, the molecule is assumed to consist of the metal and four adjacent entities. This simplification is probably justified for discussion of the ligand field transitions because the primary contributions to vibronic intensity will arise from metal–ligand vibrations. The normal vibrational modes transform as a_1, b_1, and b_2 under C_{2v} symmetry. Transitions that are pure electric dipole forbidden but are vibronically allowed are called "vibronic" transitions here. Thus, for example, the one-electron transition xy to x^2-y^2, b_1 to a_1, $^1A_1$ to $^1B_1$ is completely forbidden in z polarization, vibronically allowed in x polarization, and both dipole and vibronically allowed in y polarization.

2. Assignments. The electronic absorption spectrum consists of five major peaks in the 18 000–40 000-cm^{-1} region. Several

of these peaks contain vibronic structure. (The structure is analyzed below; vide infra.) The positions of all of these features are listed in Tables I and II. The assignments of the bands are based primarily on their polarizations.

a. The $^1A_1 \rightarrow {}^1B_1$ Transition. The most clearly resolved low-energy feature is the peak at 30 313 cm^{-1} in perpendicular polarization shown in Figure 4. This peak contains a vibronic progression of 293 cm^{-1}. In addition this peak is asymmetric with a poorly defined shoulder on the high-energy side. In parallel polarization, the 30 313-cm^{-1} peak intensity is dramatically reduced and a new maximum observed at about 31 621 cm^{-1}. On the basis of its polarization properties (and energy, vide infra), the peak at 30 313 cm^{-1} is assigned to the $^1A_1$ to $^1B_1$ transition, which is dipole allowed in perpendicular polarization and forbidden in parallel polarization.

b. The $^1A_1 \rightarrow {}^1A_2$ and the $^1A_1 \rightarrow {}^1B_2$ Transitions. The next transition toward higher energy, which appears as a shoulder on the 30 313-cm^{-1} band A, is labeled band B in Figure 4. The polarization properties of this transition cannot be unambiguously determined because it is obscured by the intense band A, but it is most evident in parallel polarization where the intensity of band A is minimized. Band B is assigned to the $^1A_1$ to $^1A_2$, d_{yz} to $d_{x^2-y^2}$ transition which is electric dipole forbidden but vibronically allowed in both parallel and perpendicular polarizations. The next clearly resolved peak toward the high-energy side of the spectrum has its maximum at 34 118 cm^{-1} in the spectrum obtained by using parallel polarization (bands C in Figure 5). This peak contains a well-resolved vibronic progression with a spacing of 348 cm^{-1}. In perpendicular polarization the intensity of the main peak is strongly decreased, revealing a new, well-resolved peak on the high-energy side at 34 600 cm^{-1} (bands D). The well-resolved peak in parallel polarization at 34 118 cm^{-1} is assigned to the $^1A_1$ to $^1B_2$ transition, which is dipole allowed in parallel polarization.

The peaks at 30 313, 31 621, and 34 118 cm^{-1} closely resemble those observed in the polarized crystal spectrum of Cossa's salt, $Pt(NH_3)Cl_3^-$.[12,13] Both the polarization properties and the energies of the peaks are similar. It is thus not surprising that our assignments of these three peaks in Zeise's salt parallel those of Martin et al.[12] for Cossa's salt.

c. Charge-Transfer Transitions. The set of peaks (bands D) centered at 34 600 cm^{-1} and allowed in perpendicular polarization consists of a four-membered vibronic progression. No analogues to this peak or any of the other peaks observed in Zeise's salt are found in the spectrum of Cossa's salt.[12] One of the major differences in electronic structure between the two compounds is the presence of empty π antibonding orbitals in Zeise's salt. Thus, the high-energy features in Figure 5 are readily assigned to platinum to olefin charge-transfer transitions. The extinction coefficient for the 34 600-cm^{-1} peak measured in the solution spectrum is less than 10^3 L/(mol cm). On the basis of the extinction coefficient, this peak is assigned to a spin-forbidden metal to ligand charge transfer. On the basis of the orbital ordering determined from the ligand field bands assigned above, band E is assigned to the platinum d_{xy} to olefin π^*, $^1A_1$ to $^3A_2$ transition. The polarization properties of triplet states are quite different from those of singlet states of the same orbital symmetry. The $^3A_2$ state transforms as A_1, B_1, and B_2 in the C_{2v} double group. Components of this state will be allowed in all polarizations. The intensity of the transition to the $^3A_2$ state will be governed by its spin–orbit coupling to spin-allowed states. For these reasons, the experimentally observed perpendicular polarization cannot be used to assign the state. As will be discussed later, the assignment is consistent with the ligand field parameters.

The remaining peak in the high-energy region (labeled E in Figure 3) occurs at 35 739 cm^{-1}. It is assigned to the $^1A_1$ to $^3B_1$, d_{yz} to olefin π^* transition on the basis of the metal d orbital ordering determined from the ligand field bands.

d. Spin-Forbidden Bands. In addition to the well-defined peaks and shoulders discussed above, broad, weak features are observed in the low-energy region below 28 000 cm^{-1}. These features are transitions to the spin-forbidden ligand field states of predominently triplet character. Because only several unresolved absorption bands corresponding to nine possible transitions are observed, assignments of the ligand field triplet states would be speculative and will not be attempted.

3. Vibronic Structure. a. Assignments. The vibronic structure observed on the absorption bands arises primarily from totally symmetric metal–ligand stretching vibrations whose frequencies have been reduced from those in the ground state. The longest progression was observed on the $^1B_1$ band with a spacing of 293 cm^{-1}. (The vibronic spacings were analyzed by using derivative spectra.) This vibronic progression probably arises from the primarily trans Cl–Pt–Cl stretching mode, whose ground-state value is 331 cm^{-1}.[14] The vibrational frequency of the excited state is reduced by about 40 cm^{-1} compared with that in the ground state. In K_2PtCl_4 the totally symmetric Pt–Cl stretch in the excited state is reduced to 290 cm^{-1} from the ground-state value of 329 cm^{-1}, also a change of about 40 cm^{-1}.[15]

Five vibronic bands are observed on the $^1B_2$ ligand field band. The observed spacing is 348 cm^{-1}. This spacing could arise from the totally symmetric platinum–olefin stretch reduced by 62 cm^{-1} from its ground-state value of 410 cm^{-1}. This d_{xz} to $d_{x^2-y^2}$ transition weakens both the π and σ metal–olefin bonds.

Four vibronic bands are observed on the $^3A_2$ charge-transfer band. The observed spacing is 788 cm^{-1}. This energy spacing is much larger than any of the metal–ligand stretching or bending energies. In the ground state, the normal modes closest in energy are the 720-, 841-, and 975-cm^{-1} CH_2 modes.[14] The ground-state C=C stretch, which might be expected to couple to the metal to ligand charge-transfer transition, is found at 1515 cm^{-1}.[16] Because the observed vibronic frequency is larger than the metal–ligand modes, it is reasonable to assign the peaks to an ethylene-centered normal mode. If the MIME effect occur in any of the progressions discussed above, the observed spacings could arise from a mixture of many normal modes.[17]

b. Excited-State Distortions in the $^1A_1$ to $^1B_1$ Transition. The vibronic structure on the $^1B_1$ peak can be used in a Franck–Condon analysis to determine the excited-state bond lengthening.[15] Because the origin of the transition is obscured by low-intensity spin-forbidden transitions, a relatively large error limit of ±0.04 Å is assigned. The relative intensities of the vibronic components are given by

$$\frac{I_{abs}m,0}{I_{abs}0,0} = \left(\frac{E_{m,0}}{E_{0,0}}\right)^1\left(\frac{R_{m,0}}{R_{0,0}}\right)^2 \quad (1)$$

The frequency dependence is

$$\left(\frac{E_{m,0}}{E_{0,0}}\right) = \frac{E_{0,0} + mh\nu_0'}{E_{0,0}} \quad (2)$$

where $E_{0,0}$ is the energy of the electronic transition between the $v' = v'' = 0$ vibrational levels and ν_0'' and ν_0' are the eigenfrequencies of the oscillator in the electronic ground and excited states. The vibrational overlap integrals have been evaluated for harmonic oscillator wave functions. The most useful relations are given by

$$R_{0,0} = [2\delta/(1 + \delta^2)]^{1/2} \exp(-\tfrac{1}{2}\rho^2) \quad (3)$$

$$R_{n+1,0} = \frac{-2\delta D R_{n,0} - (2n)^{1/2}(\delta^2 - 1)R_{n-1,0}}{(\delta^2 + 1)[2(n + 1)]^{1/2}} \quad (4)$$

where $\delta = (\nu_0'/\nu_0'')^{1/2}$, $D = C(m\nu_0')^{1/2}\Delta S$, and $\rho = D/(1 + \delta^2)^{1/2}$. When the displacement ΔS of the minimum of the potential

(12) Fanwick, P. E.; Martin, D. S. *Inorg. Chem.* **1973**, *12*, 24.
(13) Francke, E.; Moncuit, C. *Theor. Chim. Acta* **1973**, *29*, 319.
(14) (a) Adams, D. M. "Metal-Ligand and Related Vibrations"; Arnold Ltd.: London, 1967; p 73. (b) Hiraishi, J. *Spectrochim. Acta Part A* **1969**, *25*, 749.
(15) Yersin, H.; Otto, H.; Zink, J. I.; Gliemann, G. *J. Am. Chem. Soc.* **1980**, *102*, 951.
(16) Reference 14a, p 209.
(17) Tutt, L.; Tannor, D.; Heller, E. J.; Zink, J. I. *Inorg. Chem.* **1982**, *21*, 3858.

surface of the excited electronic state along the stretching normal coordinate S is expressed in Å, the vibrational energy in cm^{-1}, and the masses from the G matrix in amu's, the constant takes the value $C = 0.1722$.

The best-fit value of ΔS is 0.23 Å in the cis Pt–Cl totally symmetric normal mode using the ground-state vibrational frequency of 308 cm^{-1} and the excited electronic-state vibrational frequency of 267 cm^{-1}. The 0.23-Å distortion in Zeise's salt is very similar to the 0.20 Å distortion calculated for K_2PtCl_4.

4. Ligand-Field Analysis and Parameters. Electronic spectra of square-planar platinum ions have been interpreted by using the crystal field parameters Dq, Ds, and Dt[18-20] and the angular overlap parameters l_σ and l_π.[13,21,22] The angular overlap parameters provide more chemical insight and will be used to interpret the spectrum of Zeise's salt. The l_σ and l_π parameters for the chloride ligands are assumed to be the same for each chloride. This approximation is quite reasonable because the crystallographically determined cis and trans Pt–Cl bond lengths differ by only 2%. The l_π parameter for the olefin is assumed to be zero in the xy plane; i.e., only π interactions involving the olefin π antibonding orbital and the metal d_{xz} orbital are assumed to contribute. This assumption would be rigorous in perfect C_{2v} symmetry.

The energies of the spin-allowed ligand field transitions are given by eq 5–8,

$$-C + (9/4)l\sigma^{Cl} + (3/4)l\sigma^{cc} - 3l\pi^{Cl} = \Delta E(^1B_1) \quad (5)$$

$$-3B - C + (9/4)l\sigma^{Cl} + (3/4)l\sigma^{cc} - 2l\pi^{Cl} = \Delta E(^1A_2) \quad (6)$$

$$-3B - C + (9/4)l\sigma^{Cl} + (3/4)l\sigma^{cc} - l\pi^{Cl} - l\pi^{cc} = \Delta E(^1B_2) \quad (7)$$

$$-4B - C + (6/4)l\sigma^{Cl} + (2/4)l\sigma^{cc} = \Delta E(^1A_1) \quad (8)$$

where B and C are Racah electron–electron repulsion parameters and the cc and Cl superscripts on the angular overlap parameters refer to the ethylene and chloride ligands, respectively.

Because there are more parameters than observed transitions, it is impossible to obtain a unique solution for the parameters. However, several assumptions can be made to severly restrict the parameters and provide a narrow range of solutions that allow the σ and π bonding of ethylene to be reliably compared to other ligands.

The simplest starting point is to assume that all of the parameters obtained from $PtCl_4^{2-}$ are transferrable to Zeise's salt. There are then only two adjustable parameters and three transitions. Using $l\sigma^{Cl}$ = 12 420 cm^{-1}, $1\pi^{Cl}$ = 2800 cm^{-1}, B = 600 cm^{-1}, C = 2400 cm^{-1}, and eq 1 and 3, we calculate l_σ^{cc} = 17 829 cm^{-1} and $l\pi^{cc}$ = 199 cm^{-1}.

An alternative analysis proceeds in three steps. First, from eq 5 and 6, the energy difference between the $^1B_1$ and $^1A_2$ bands is given by

$$l_\pi^{Cl} - 3B = 925 \text{ cm}^{-1} \quad (9)$$

If it is assumed that the l_π^{Cl} value determined from $PtCl_4^{2-}$ is transferrable to Zeise's salt, then B = 497 cm^{-1}. This value is between those reported for $PtCl_4^{2-}$ (i.e., between 330 and 600 cm^{-1}). When this B value of 497 cm^{-1} is used and $C = 4B$ is assumed as usual, the value of l_σ^{cc} calculated from eq 5 is l_σ^{cc} = 17 008 cm^{-1}. As a check, l_σ^{cc} can be calculated using eq 6, yielding the identical value. By use of the above values and eq 7, l_π^{cc} = 286 cm^{-1}.

The two calculations discussed above yield angular overlap parameters that agree to within a few percent. The parameters are compared to those calculated for $PtCl_4^{2-}$ and $PtCl_3NH_3^-$ in Table IV. The two-dimensional spectrochemical series for platinum(II) based on transferrable parameters for the chloride ligand is shown in Figure 7.

Table IV. Ligand-Field Parameters for $PtCl_3L^{n-}$

L	B	C	l_σ^{Cl}	l_π^{Cl}	l_σ^{L}	l_π^{L}
Cl^- [a]	330	560	11 510	2130		
	600	2400	12 420	2800		
NH_3	600	2400	12 420	2800	15 620	1700
C_2H_4 [b]	600	2400	12 420	2800	17 557	−5
C_2H_4 [c]	497	1988	12 420	2800	17 008	286

[a] The two values listed represent the high and low values from the literature. [b] Calculated by using the chloride parameters from K_2PtCl_4. [c] Calculated as discussed in the text.

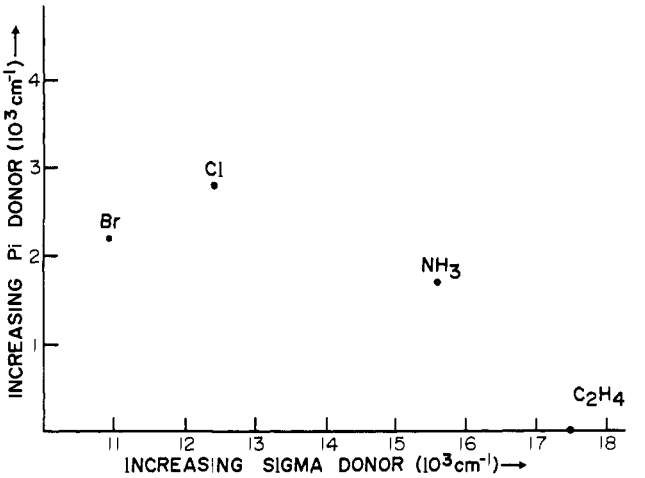

Figure 7. Two-dimensional spectrochemical series for ligands bonded to the Cl_3Pt^- unit.

5. Olefin–Metal Bonding Properties. The most striking result of the ligand field analysis is the surprisingly large σ interaction between platinum and ethylene. Ethylene is a better σ donor than ammonia. This conclusion is readily apparent from the spectrum. The position of the $^1B_1$ state, which was unambiguously assigned, is primarily determined by l_σ^{cc} and l_σ^{Cl}. Its position in the spectrum of Zeise's salt is higher in energy than the $^1B_1$ band in $PtCl_3NH_3^-$. Thus the position of ethylene in the σ portion of the two-dimensional spectrochemical series is higher than that of ammonia.

The π interaction parameter for ethylene shows that it is a weak π acceptor ligand. The numerical value of $l\pi^{cc}$ is more sensitive to the approximations used in its calculation than in l_σ^{cc}. Thus the experimental uncertainty is larger. The value for l_π^{cc} given in Table IV indicates that it is a better π acceptor (weaker π donor) than chloride. Given the error limits of l_π^{cc}, we hesitate to offer detailed comparisons of the ligand's π bonding capabilities. It is safe to conclude that ethylene is a π acceptor in the two-dimensional spectrochemical series.

The relative importances of σ and π interactions have previously been investigated by using kinetic, thermodynamic, and NMR data. In a comprehensive report, Tolman suggested that the importance of the π interaction will vary with the HOMO of the metal and will decrease in the order Ni(0) > Rh(I) > Pt(II) > Ag(I).[23] In the case of Ni(0), where π effects should be very strong, he found a good correlation between metal–olefin stability and the LUMO of the free olefin. In contrast, Venanzi et al.[24,25] and Partenheimer et al.[26] found that electron-donating groups on the olefin lower the displacement energies of the olefins from Pt(II). These results suggest that π effects are dominant. However, Tolman noted that there is appreciable reorganization energy when the olefin binds to the metal and that electronic data are needed for the distorted olefin. The electronic spectroscopic data reported in this paper clearly show that in the complex in

(18) Fenske, R. F.; Martin, D. S.; Ruedenberg, K. *Inorg. Chem.* **1962**, *1*, 441.
(19) Martin, D. S.; Tucker, M. A.; Kassman, A. J. *Inorg. Chem.* **1965**, *4*, 1682.
(20) Tuszynski, W.; Gliemann, G., *Z. Naturforsch. A* **1979**, *34A*, 211.
(21) Jorgensen, C. F.; Pappalardo, R.; Schmidtke, H. H. *J. Chem. Phys.* **1963**, *39*, 1422. Schaffer, C. F.; Jorgensen, C. K. *Mol. Phys.*, **1965**, *9*, 401.
(22) Vanquickenborne, L. G.; Ceulemans, A. *Inorg. Chem.* **1981**, *20*, 796.
(23) Tolman, C. A. *J. Am. Chem. Soc.* **1974**, *96*, 2780.
(24) Hartley, F. R.; Venanzi, L. M. *J. Chem. Soc. A* **1967**, 330.
(25) Denning, R. G.; Venanzi, L. M. *J. Chem. Soc. A* **1967**, 336.
(26) Partenheimer, W. *J. Am. Chem. Soc.* **1976**, *98*, 2779.

its actual geometric arrangement *the σ interaction between the olefin and the metal d orbitals is significantly more important than the π interaction with the d orbitals.*

Three types of molecular orbital calculations have been carried out to assess the relative σ and π bonding in Zeise's salt. An extended Hückel calculation concluded that σ and π bonding were of about equal importance.[4] The same conclusion was reached on the basis of a CNDO type calculation.[5] An Xα-SW calculation concluded that the π bonding is much less than the π bonding.[6] Because the transition energies calculated in these studies were all so far from those experimentally observed, the above conclusions are not of quantitative use.

6. Photochemical Consequences. The solution-phase photochemistry of Zeise's salt has been studied by Adamson et al.[27] The onset of photoreactivity began at about 26 000 cm^{-1} and reached the highest quantum yields for ligand substitution at 32 800 cm^{-1}. The authors attributed the ethylene aquation photoreaction to the lowest-energy singlet state.

The detailed assignment of the spectrum of Zeise's salt provides a straightforward, a posteriori interpretation of the photochemistry. The lowest ligand field transition populates the $d_{x^2-y^2}$ orbital. This orbital is most strongly σ antibonding between the platinum and the ethylene ligand, as shown by the l_σ parameters in Table IV.

(27) Natarajan, P.; Adamson, A. W., *J. Am. Chem. Soc.* **1971**, *93*, 5599.

The photochemical loss of ethylene is thus most simply interpreted in terms of the large σ bond weakening between the platinum and ethylene in the excited state. The π-bonding changes in the excited state reinforce the bonding explanation of the photochemistry. The d_{xy} orbital which is depopulated in the lowest ligand field transition is π antibonding between the platinum and the chloride ligands. Thus the one-electron transition depopulates a π-antibonding orbital which strengthens the metal chloride π bonds. The major orbital factor governing the photochemistry is the population of the $d_{x^2-y^2}$ orbital, which is σ antibonding between the platinum and the ethylene.

Summary

Ligand field and charge-transfer electronic absorption transitions have been assigned in the low-temperature single-crystal polarized absorption spectrum. The lowest energy ligand field excited state arises from the d_{xy} to $d_{x^2-y^2}$ one-electron transition. This excited state undergoes a 0.23-Å distortion in the totally symmetric cis Pt-Cl stretching normal mode. Angular overlap parameters were determined. Ethylene is a strong σ donor (stronger than ammonia) and a weak π acceptor toward Pt(II).

Acknowledgment. The support of the National Science Foundation is gratefully acknowledged.

Registry No. Zeise's salt, 16405-35-9.

Localization and Transfer of Protons between ^{15}N Atoms of *meso*-Tetraphenylporphine Probed by Nuclear Overhauser Effects and Dipole-Dipole Relaxation Times

Jürgen Hennig and Hans-Heinrich Limbach*

Contribution from the Institut für Physikalische Chemie der Universität Freiburg i.Br., D-7800 Freiburg, West Germany. *Received December 27, 1982*

Abstract: The longitudinal relaxation times T_1 of the central and of the β-pyrrole protons of $^{15}N_4$-*meso*-tetraphenylporphine (TPP) dissolved in toluene-d_8 have been measured at 90.02 MHz, and the ^{15}N-T_1, including the Nuclear Overhauser Effects (NOE), at 9.12 MHz, both as a function of the temperature. A ^1H-T_1 minimum was observed at approximately 220 K. The data for the central protons could be explained by a superposition of two dipolar relaxation mechanisms, one involving the ^{15}NH and the other the central HH dipolar pair. The β-pyrrole proton data were consistent with a mutual dipolar relaxation mechanism of these protons. Below room temperature the thermally activated hydrogen tunneling process of the inner protons between the four nitrogen atoms is slow and the ^{15}N NMR spectra show two ^{15}N signals which arise from the protonated and the nonprotonated nitrogen atoms in accordance with the literature. Because of the proton exchange, these two signals have the same T_1 and the same negative NOE above 200 K. At lower temperatures, slow proton exchange causes an NOE breakdown of the nonprotonated nitrogen signal which is accompanied by different T_1 values for the two signals. The NOE of the NH signal breaks down at a lower temperature because of slow molecular tumbling. The Arrhenius curve of the hydrogen migration previously determined could be verified also at lower temperatures by a quantitative calculation of the NOE as a function of temperature. The protonated nitrogen is relaxed by dipole-dipole coupling to the inner proton. The intrinsic relaxation of the nonprotonated nitrogen could be described to a major extent by the chemical shift anisotropy relaxation mechanism and to a minor extent by direct dipole-dipole relaxation to the distant inner protons which yields a small negative NOE. Vibrationally averaged mean cubic distances of 1.02 Å for the inner NH bond and of 2.4 Å for the distance between the central protons, as well as a distance of about 2.5 Å between two closest β-pyrrole protons, were derived from the relaxation data without assumptions concerning the anisotropy of the molecular tumbling. The possibility of detecting small amounts of tautomers by NOE measurements is discussed.

Introduction

The problem of proton localization and transfer in hydrogen bonded systems is a matter of continuing theoretical and experimental interest.[1-24] In particular, the hydrogen migration in *meso*-tetraphenylporphine (TPP)[1-12] has attracted special attention.

(1) Limbach, H. H. "The Use of NMR Spectroscopy in the Study of Hydrogen Bonding in Solution", in "Aggregation Processes", Gormally, J.; Wyn-Jones, E., Ed., Elsevier: Amsterdam, 1983; Chapter 16.

(2) Storm, C. B.; Teklu, Y. *J. Am. Chem. Soc.* **1974**, *94*, 53. Storm, C. B.; Teklu, Y. *Ann. N.Y. Acad. Sci.* **1973**, *206*, 631.

(3) Abraham, R. J.; Hawkes, G. E.; Smith, K. M. *Tetrahedron Lett.* **1974**, 1483.

(4) Eaton, S. S.; Eaton, G. R. *J. Am. Chem. Soc.* **1977**, *99*, 1601.

(5) Gust, D.; Roberts, J. D. *J. Am. Chem. Soc.* **1977**, *99*, 3637.

0002-7863/84/1506-0292$01.50/0